Spatiotemporal Characterization of Extracellular Matrix Microstructures in Engineered Tissue: A Whole-Field Spectroscopic Imaging Approach

Zhengbin Xu
Weldon School of Biomedical Engineering,
Purdue University,
West Lafayette, IN 47907

Altug Ozcelikkale
School of Mechanical Engineering,
Purdue University,
West Lafayette, IN 47907

Young L. Kim[1]
Weldon School of Biomedical Engineering,
Purdue University,
West Lafayette, IN 47907
e-mail: youngkim@purdue.edu

Bumsoo Han[1]
School of Mechanical Engineering,
and Weldon School of Biomedical Engineering,
Purdue University,
West Lafayette, IN 47907
e-mail: bumsoo@purdue.edu

Quality and functionality of engineered tissues are closely related to the microstructures and integrity of their extracellular matrix (ECM). However, currently available methods for characterizing ECM structures are often labor-intensive, destructive, and limited to a small fraction of the total area. These methods are also inappropriate for assessing temporal variations in ECM structures. In this study, to overcome these limitations and challenges, we propose an elastic light scattering approach to spatiotemporally assess ECM microstructures in a relatively large area in a nondestructive manner. To demonstrate its feasibility, we analyze spectroscopic imaging data obtained from acellular collagen scaffolds and dermal equivalents as model ECM structures. For spatial characterization, acellular scaffolds are examined after a freeze/thaw process mimicking a cryopreservation procedure to quantify freezing-induced structural changes in the collagen matrix. We further analyze spatial and temporal changes in ECM structures during cell-driven compaction in dermal equivalents. The results show that spectral dependence of light elastically backscattered from engineered tissue is sensitively associated with alterations in ECM microstructures. In particular, a spectral decay rate over the wavelength can serve as an indicator for the pore size changes in ECM structures, which are at nanometer scale. A decrease in the spectral decay rate suggests enlarged pore sizes of ECM structures. The combination of this approach with a whole-field imaging platform further allows visualization of spatial heterogeneity of EMC microstructures in engineered tissues. This demonstrates the feasibility of the proposed method that nano- and micrometer scale alteration of the ECM structure can be detected and visualized at a whole-field level. Thus, we envision that this spectroscopic imaging approach could potentially serve as an effective characterization tool to nondestructively, accurately, and rapidly quantify ECM microstructures in engineered tissue in a large area. [DOI: 10.1115/1.4024130]

Introduction

Microstructures and integrity of the ECM of engineered tissue are critical to their quality and functionality [1–3]. Moreover, decellularized ECM scaffolds have also received considerable attention as a promising approach for engineering functional organ replacement [4,5]. Thus, quantitative assessments of the ECM and scaffold microstructures are of great significance for tissue engineering and regenerative medicine. However, currently available assessment methods, such as electron microscopy, optical microscopy, and equilibrium swelling, are often labor-intensive and destructive. Any assays using exogenous probes also reduce usable volumes of tissue and further require toxicity tests for *in vivo* implantation. In addition, a better understanding of the dynamic nature of ECM microstructures originating from cell-ECM interactions and matrix remodeling is critical to generate biomimetic tissue constructs [6]. Using conventional methods, it is, however, challenging to characterize spatiotemporal changes in ECM microstructures.

Besides research and scientific purposes, rapid and high-throughput assessments of the ECM or scaffold microstructures are highly relevant to quality control of engineered tissue in industrial and clinical settings. For example, cryopreservation of engineered tissue has been actively pursued to provide reliable long-term storage and off-the-shelf availability of cell/tissue engineering products for clinical use. Since many of the functional properties of tissue are associated with ECM microstructures, post-thaw ECM microstructures can be a crucial marker for the functionality of the post-thaw tissue. Recent studies reported that ECM microstructures could be affected by freezing-induced cell-fluid-matrix interactions [3,7]. Thus, rapid and nondestructive assessments of post-thaw ECM structures can be valuable tools to confirm quality of cryopreserved tissue prior to their use. Moreover, engineered tissue in clinically relevant size is large, but conventional bioassays and imaging methods can only evaluate a small fraction of the total area. Conventional methods require a large number of images to be stitched together to cover a large tissue area, which can be computationally intensive and time-consuming.

To address these challenges, we propose a new imaging method on the basis of an elastic light scattering approach. The underlying rationale is that elastic light scattering spectra (i.e., scattering without change in the wavelength) are sensitive to scattering structures in size comparable to the wavelength [8–10]. The principle of this method is that the spectral pattern of light elastically reflected from tissue is determined by the structures of light scatterers. In particular, spectral behavior of elastic light scattering depends on the size distribution of scatterers. Typically, the light scattering spectrum from biological tissue is a declining function of the wavelength and its steepness depends on the overall size distribution of scattering microstructures. Larger structures generally yield slower declining spectra, while smaller structures tend

[1]Corresponding authors.

Manuscript received October 23, 2012; final manuscript received March 28, 2013; published online July 11, 2013. Assoc. Editor: Liang Zhu.

to increase the steepness of the decline. Spectral patterns of elastic light scattering have been intensively used to detect cancer [10–12]. It was also demonstrated that a light scattering approach could capture nanoscale prefailure deformation of bone at extremely low strains [13].

In this study, we employ this approach to spatiotemporally characterize ECM microstructures in engineered tissue. Specifically, it is tested whether spectroscopic measurements of light elastically backscattered from engineered tissue can be correlated to ECM structural changes. First, we combine this approach with a whole-field spectroscopic imaging platform to demonstrate the feasibility for a nondestructive, whole-field, and sensitive spatiotemporal characterization method. Acellular collagen scaffolds and dermal equivalents (i.e., fibroblast-embedded collagen gels) are used as model ECM structures. Second, backscattering spectra from collagen scaffolds are obtained and analyzed to characterize microstructural alterations in the collagen matrix due to collagen concentration and freezing-induced structural changes. Third, spatiotemporal changes in ECM structures during cell-driven compaction are assessed using dermal equivalents. Finally, we discuss the potential utilization of the proposed imaging approach for ECM microstructure characterization in engineered tissue.

Materials and Methods

Cells and Reagents. Early passage human dermal fibroblasts were maintained in a culture medium (DMEM/F12, Invitrogen, Grand Island, NY) supplemented with 10% fetal bovine serum, 2 mM L-glutamine, and 100 mg/ml penicillin/streptomycin. The fibroblasts were cultured up to the 15th passage in 75 cm^2 T-flasks at 37 °C and 5% CO_2. The cells were consistently harvested at 80% confluency by using 0.05% trypsin and 0.53 mM ethylenediamine tetra-acetic acid.

Experimental Design. The experimental groups were designed to create the ECM structural differences caused by (i) collagen concentration (i.e., comparison between 3 mg/ml and 6 mg/ml unfrozen gels); (ii) freezing-induced structural changes (i.e., comparison between unfrozen and frozen/thawed gels at a given collagen concentration); and (iii) cell-driven compaction (i.e., time-lapse imaging of unfrozen dermal equivalents with 3 mg/ml collagen concentration).

Collagen Matrix and Freeze/Thaw Protocol. Collagen matrices were prepared and exposed to a freeze/thaw process as described elsewhere [3,14,15]. In brief, a collagen solution of 2 ml was prepared from a high concentration type I rat tail collagen (BD Biosciences, Bedford, MA). The final collagen concentrations were 3 or 6 mg/ml. The solution contained 10% 10×MEM, 30 mM HEPES, 10 g/ml penicillin/streptomycin, 2 mM L-glutamine, 6% fetal bovine serum, and 2.3% (v/v of collagen added) 1 N sodium hydroxide. Then, distilled water was added to make a total volume of 2 ml. The collagen solution was placed in a chamber slide (Lab-Tek II, Nunc, Naperville, IL) and allowed to polymerize at 37 °C for 1 h. After polymerization, 2 ml of 1×PBS was added and the engineered tissue was incubated before the freezing procedure. The matrices were then frozen on a directional freezing stage, in which a temperature gradient was set at −20 °C to 4 °C over a 6 mm gap and passively thawed at room temperature. The matrices were incubated at 37 °C with 1×PBS for 3 h and were fixed with 3% formaldehyde prior to imaging.

Dermal Equivalent: Fibroblast-Embedded Collagen Matrix. To create spatiotemporal changes in ECM microstructures, dermal equivalents were prepared by seeding human dermal fibroblast cells in type I collagen matrix (BD Biosciences, Bedford, MA) at a collagen concentration of 3 mg/ml. The cell seeding concentration was 2×10^5 cells/ml. After the polymerization, the mixture was incubated in culture medium at 37 °C for 24 h for the cells to adhere to and grow within the collagen matrix. After 24-h culture, the dermal equivalents were imaged under the spectroscopic imaging setup.

Elastic Light Scattering-Based Spectroscopic Imaging Setup. Figure 1 illustrates our spectroscopic imaging system described elsewhere [13,16,17]. In brief, a beam from the xenon arc lamp was collimated using a four focal length (4-f) system and delivered onto the specimen through the beamsplitter. The backscattered light traveled back through the beamsplitter and was collected within a small angular cone of 2 deg via the second 4-f system (i.e., back-directional gating). This backscattered light went into the slit of the spectrograph located on the image plane and was further separated into various wavelengths. The imaging system also had a long working distance approximately 30 mm for noncontact and noninvasive imaging. A CCD camera mounted on the spectrograph captured the separated light and recorded a matrix of intensity as a function of pixel locations x, y, and wavelength λ (=400 nm–700 nm). In the imaging platform, cross-talk between adjacent pixels can be minimized to enhance the image contrast and resolution, because back-directional gating can significantly suppress diffuse light in biological tissue [17]. In this study, the specimens were imaged in an area of 13 mm × 12 mm with a pixel size of 50 μm. Overall, the imaging setup allowed to obtain intensity matrices as a function of x, y, and λ. The (x, y) data components provide planar images in 2D while the λ data component allows us to extract the microstructural information as described below.

Spectral Analysis and Image Construction. Different declining functions over the wavelength can be utilized to characterize spectral variations. Inverse power-law spectral component, exponential decay, and simple linear declining function were successfully used to infer submicron structures of scattering media [10,18]. Indeed, this simple approach has been intensively used for characterizing tissue structures. For example, linear spectral slope, serving as an easily obtainable biomarker, was used to differentiate precancerous stages in animal models of colon carcinogenesis [12]. In a recent study, it was demonstrated that a linear spectral decay function can be used to visualize heterogeneous prefailure deformation of bone [13]. Similarly, we hypothesize that spectral dependence of light elastically scattered from tissue scaffolds and constructs can be used to probe alterations in ECM microstructures. Because the developed spectroscopic imaging system generated an intensity data set as a function of x, y, and λ, a spectral pattern at each (x, y) position can be examined. To account for spectral variations at each pixel, the backscattered intensity was fitted to an exponential decay over the wavelength

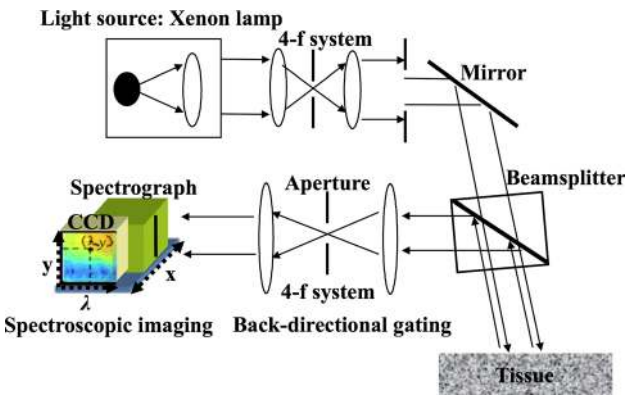

Fig. 1 Schematic diagram of the spectroscopic imaging setup. This system obtains three-dimensional data sets as a function of (x, y, λ). Back-directional gating in the imaging arm significantly reduces cross-talk among adjacent (x, y) locations and allows large-area imaging.

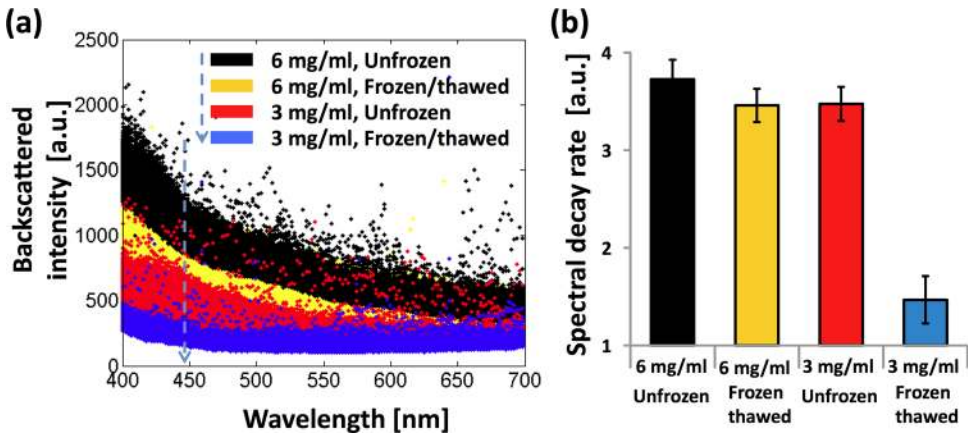

Fig. 2 (*a*) Representative spectra of elastically backscattered light from unfrozen and frozen/thawed regions of each collagen scaffold. (*b*) Comparison of spectral decay rates β for each scaffold region. Error bar represents standard deviations ($n \geq 3$ for all data points).

such that $I(\lambda) = \alpha \exp(-\beta \lambda)$, where α and β are constants. The value of β (hereafter referred as a spectral decay rate) at each (x, y) location was used to form 2D planar spectroscopic images. In order to assess the freezing-induced structural changes in the collagen matrices, the region near the interface of unfrozen and frozen/thawed parts was imaged simultaneously. To obtain time-lapse images, the dermal equivalents were placed under the imaging setup after 24 h incubation and imaged for 2.5 h in a 30-min interval (i.e., 24–26.5 h after cell seeding). During all imaging sessions, the collagen matrices and dermal equivalents were placed in 1×PBS solutions to prevent dehydration.

Scanning Electron Microscopy (SEM). The microstructures of collagen scaffolds were assessed using quantitative SEM as described previously [3,14,15]. In brief, specimens were fixed with 2% tannic acid and cut into 3 mm diameter disks. The disks were stained with 2% uranyl acetate, and then encapsulated in wet-SEM sample holders (QX-302 capsule, Quantomix, Hartfield, PA) with buffering solution (QX-302 imaging buffer, Quantomix). The specimens were imaged under the hydrated state using a scanning electron microscope (JSM-35C, JEOL, Tokyo, Japan). The SEM micrographs were quantitatively analyzed using NIH ImageJ for mean void area ratio as described elsewhere [14,15,19]. Briefly, at least 5 interrogation windows of 150×150 pixels were randomly cropped and despeckled. The interrogation windows were then binarized and skeletonized. The number of pixels occupied with voids was obtained and normalized to the total number of pixels.

Microstructures of dermal equivalents were also visualized using a cryo-SEM technique. The dermal equivalents were fixed and stained with tannic acid and uranyl acetate, and then were put into a slit insert in a sample holder. The holder was plunged into liquid nitrogen slush and the specimens were transferred to a prechamber (Gatan Alto 2500). After the specimens were fractured by a cooled scalpel to produce a free-break surface, they were sublimated followed by sputter coating with platinum and then transferred to the microscope cryostage for imaging. The specimens were imaged with an FEI NOVA nanoSEM field emission scanning electron microscope (FEI company, Hillsboro, OR) using the ET (Everhart–Thornley) detector.

Results

Figure 2(*a*) shows representative spectra from ~10,000 (x, y) pixel locations from each specimen. While the light scattering spectra from biological tissue are complex with the scale of spectral features as small as only a few nanometers [20,21], typically spectral signals are a declining function of the wavelength and its steepness depends on the overall size distribution of internal structures contributing to the spectral backscatters. As discussed, the backscattered intensity decreases with the wavelength for all of the specimens. The extent of the spectral decay appeared to depend on the ECM microstructures: the fastest decay was observed from the unfrozen 6 mg/ml collagen matrix, in which the ECM structures had smallest pores among the matrices studied. At the same collagen concentration of 3 mg/ml, the frozen/thawed matrices had a slower decay than that of the adjacent unfrozen matrix. This should be attributable to freezing-induced ECM structural changes as reported elsewhere [3,7,14]. The declining spectra can be curve-fitted to exponential decay functions over the wavelength. An averaged R^2 value was 0.76, supporting the idea that the exponential decay function can capture the major spectral variations. The quantified spectral decay rate β from 10,000 pixels in each region is shown in Fig. 2(*b*). For the unfrozen matrices, the averaged spectral decay rates increase with the collagen concentration (p-value < 0.001 adjusted for multiple comparisons using a Bonferroni correction). The averaged spectral decay rates significantly decrease after the freeze/thaw process, which indicates that freezing-induced structural changes can easily be detected by the proposed method (p-value < 0.001 adjusted for multiple comparisons using a Bonferroni correction).

Figures 3(*a*)–3(*c*) present representative SEM images of the acellular collagen scaffolds. Among the unfrozen specimens, the scaffold with the higher collagen concentration (i.e., 6-mg/ml scaffold) shows much denser microstructures than the 3-mg/ml scaffold as expected. Due to the higher amount of collagen available during the polymerization process, the porosity and pore size of the 6-mg/ml scaffold are smaller than those of the 3-mg/ml scaffold. As summarized in Fig. 3(*d*), the mean void area, which is a 2D projected porosity assessment, also confirms this observation. When the scaffold underwent a freeze/thaw process, the pore structures significantly enlarged and the matrix structures became coarse as shown in Fig. 3(*c*). The similar trends have already been reported [3,14]. These structural changes are thought to be caused by freezing-induced fluid-structure interactions [14], which are initiated by the volumetric expansion of the interstitial fluid during freezing. As a result, the mean void area increases after a freeze/thaw process (Fig. 3(*d*)).

We further correlated the spectral decay rate β with the mean void area obtained from SEM images. As the mean void area increases, the spectral decay rate β decreases as shown in Fig. 3(*e*). The correlation coefficient between the mean void area and the spectral decay rate β is ~0.978. This high value of correlation coefficient supports the approach that the spectral dependence is linearly associated with the mean void area, which is a representative assessment of porous ECM microstructures.

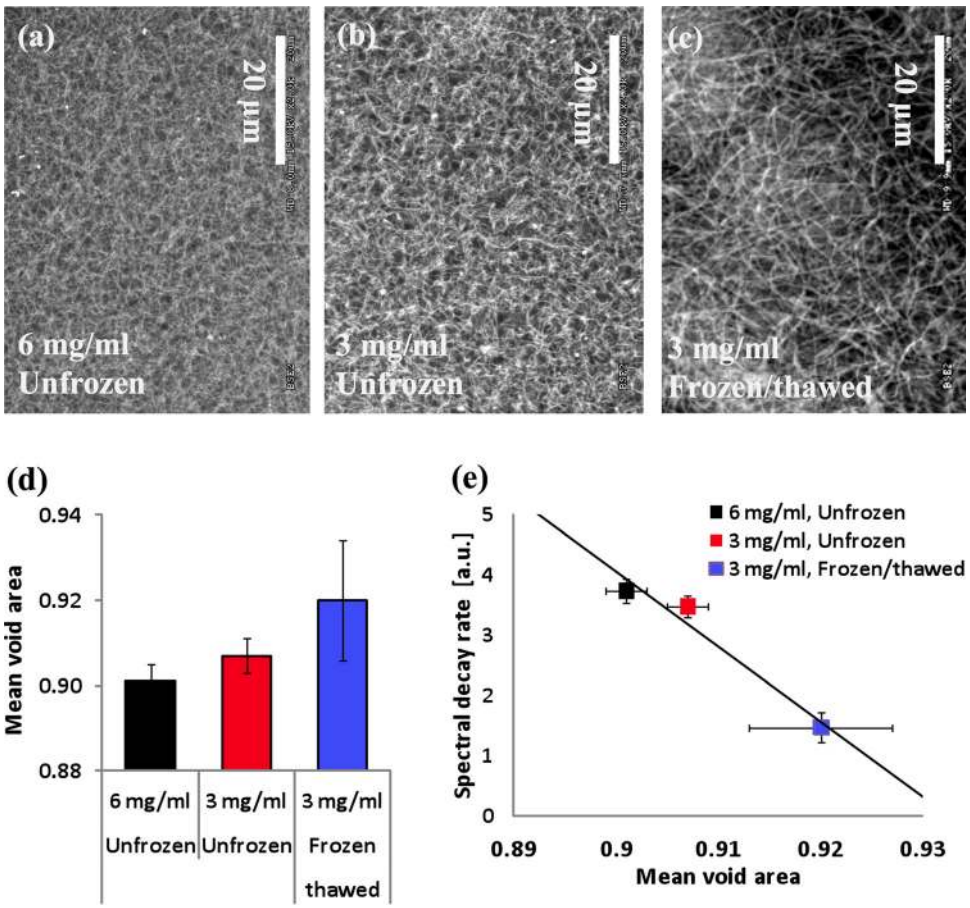

Fig. 3 (*a*)–(*c*) Representative SEM images of the scaffold microstructures from unfrozen and frozen/thawed regions. (*d*) Comparison of mean void areas for each scaffold region. (*e*) Correlation between the mean void areas and the spectral decay rates β for three distinct cases. Error bar represents standard deviations ($n \geq 3$ for all data points).

Thus, the spectral decay rate β could potentially serve as an ECM structural indicator for engineered tissue. The spectral signals are possibly affected by various properties of tissue microstructures, such as pore size, fiber diameter and orientation. A major origin of the scattering signals obtained from the imaging method is likely to link to changes in pore sizes, although other structural changes might minimally be attributable to the imaging contrast. The length scale of pore sizes is significantly greater than that of fibers, dominating the light scattering signals. The fiber orientation is unlikely to be highly sensitive, because the system configuration does not include any polarization sensitive detection. Thus, although further detailed investigation using rigorous analytical approaches (e.g., Mie theory) is required, the main possible origin of the spectral signals can be understood in this regard.

To further demonstrate the ability to visualize spatial heterogeneity of the ECM microstructures over a relatively large area, we used the value of spectral decay rate β at each (x, y) pixel to form 2D planar spectroscopic images. In Fig. 4(*a*), the spatial distribution of the unfrozen 6-mg/ml collagen matrix is uniform in an area of 13 mm × 12 mm. On the other hand, the spectroscopic image of the scaffold at 3 mg/ml (Fig. 4(*b*)) captures the spatial variation of freezing-induced ECM microstructural alterations. The clear decrease (bright to dark) of the spectral decay rate β depicts the boundary of unfrozen and frozen/thawed regions. As shown in the darker area, the frozen/thawed region had a much lower spectral decay rate β, providing a strong image contrast. In particular, tissue scaffolds/constructs in clinically relevant size are large and recent advances in tissue engineering also allow researchers to generate ECM heterogeneity in space, mimicking native tissue architectures. 2D planar spectral imaging can be sufficient to image spatial heterogeneity for practical and widespread characterization. It should be noted that this visualization method is not intended to generate 3D tomographic images of tissue constructs. The imaging depth, which the signal is averaged over, was assessed. The optical thickness of the imaging depth under the present imaging system is $\tau = 14$ where the intensity reaches to 0.63% (=exp(–1)) of the maximum intensity [22]. The physical imaging depth can further be estimated by converting τ to a physical thickness T ($=\tau \times ls$, where ls is the scattering pathlength of light). Using an integrating sphere method [23], the value of ls (averaged distance of one scattering event) was measured for the specimens used. For the collagen concentrations of 6 mg/ml

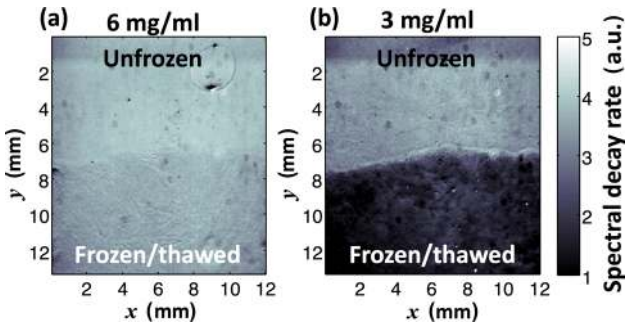

Fig. 4 Representative 2D planar spectroscopic images using the spectral decay rate β for unfrozen and frozen/thawed regions of each scaffold

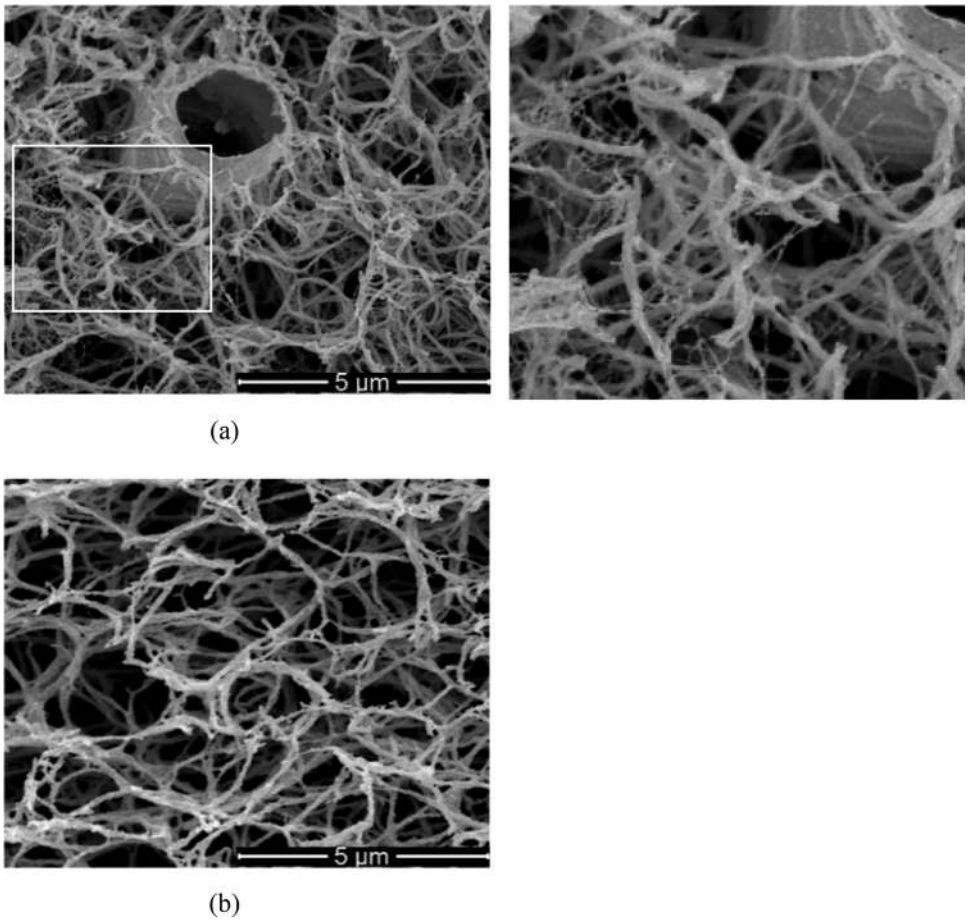

Fig. 5 Representative cryo-SEM images of engineered scaffolds. (*a*) Dermal equivalent—white area is zoomed and shown on the right. (*b*) Acellular collagen matrix. Dermal equivalent has compacted matrix structure with thinner collagen fibrils. Very fine fibril structures are observed around the cell, which is not observed in acellular matrix.

and 3 mg/ml, $ls = 0.71 \pm 0.01$ mm and $ls = 1.13 \pm 0.01$ mm, corresponding to $T = 9.94 \pm 0.14$ mm and $T = 15.82 \pm 0.14$ mm, respectively. Because the physical thickness of all the specimens used was thinner than these values, the signal from the tissue specimens was averaged over the whole thickness.

Figures 5(*a*) and 5(*b*) show representative cryo-SEM images of the dermal equivalent and the acellular collagen matrix, respectively. Several notable structural changes are observed in the ECM of the dermal equivalent. These include (1) collagen fibrils fused on the cell membrane, (2) denser ECM pore structures than the acellular matrix, (3) thinner collagen fibrils, and (4) presence of very fine new fibril structures around cells. The first two structural changes are associated with cell-ECM interactions including cell-matrix adhesion and local cell-driven compaction of the ECM. When fibroblasts interact with collagen matrices, the cells can penetrate into the matrix and become entangled with matrix fibrils [24]. The thinner collagen fibrils are thought to result from cell-driven degradation of collagen [25,26]. The very fine fibril structures around the cell, as noted in the inset of Fig. 4, are thought to be the extracellular proteins synthesized by cells, since these structures are observed only in the dermal equivalents but not in the acellular gels. Further research is warranted to confirm.

These structural changes induced by cell-ECM interaction can be confirmed by the proposed spectroscopy method. Figure 6(*a*) shows time-lapse spectroscopic images of the dermal equivalent using the spectral decay rate β. The overall value of β gradually increased over time as the spectroscopic images became brighter at later time-points. In Fig. 6(*b*), we calculated differential images by subtracting the first time-point image as the baseline. At 2.5 h after the initial imaging, the overall value of β was three times higher than the initial value. The higher values of spectral decay rates indicate smaller scattering structures within the dermal equivalent. This is thought to be caused by the cell-matrix interaction, particularly cell-driven compaction over time. Fibroblasts are well documented for their active interaction with collagen matrix within this time frame [27,28]. It is unlikely that cell proliferation contributed to the denser tissue structures, because of the relatively short period (2.5 h). Figures 6(*c*) and 6(*d*) show the time-lapse spectroscopic images of the acellular matrix over the same time period. No changes were observed in the spectral decay rate during the same time period. This supports that the present imaging method can visualize the extent of the local cell-driven compaction of the ECM.

Discussion

ECM is complex 3D microstructures of extracellular proteins, primarily collagen, providing a structural scaffold for cells to adhere and grow. In addition, its microstructural integrity is closely related to various functional properties, including the mechanical, transport, and optical properties of engineered tissue. For example, the stiffness of engineered tissue is thought to be related to the porosity of ECM and could be correlated by a power-law relationship [29]. Empirical correlations have also been proposed to correlate the diffusivity to the porosity and other structural characteristics [30,31]. Moreover, several theoretical structure–functionality relationships have been developed for transport properties including diffusivity and hydraulic

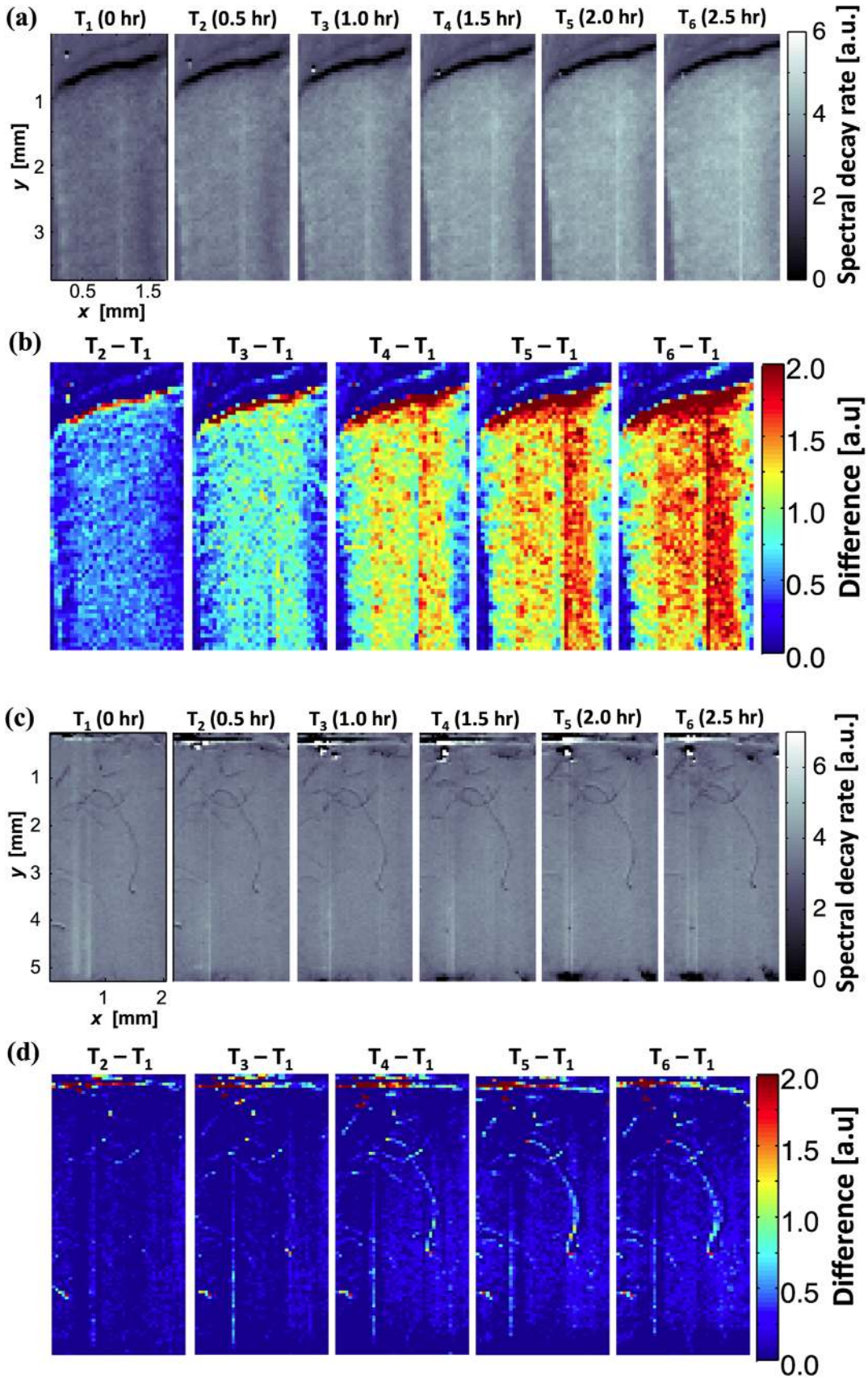

Fig. 6 Time-lapse spectroscopic images of dermal equivalent ((*a*) and (*b*)) and acellular matrix ((*c*) and (*d*)) for 2.5 h time period. (*a*) The spectral decay rate β increases over time. (*b*) Pseudocolor spectroscopic images after subtracting the image at the initial time-point (T1). The red color represents locally dense ECM structure, which is thought to be caused by the cell-driven compaction. (*c*) and (*d*) The spectral signal from acellular matrix showed no change over the same time period.

permeability. The diffusivity of hydrogels has been predicted as a product of several factors, which account for hydrodynamic and tortuosity effects separately [32,33]. These factors relate the diffusivity and hydraulic permeability of hydrogels with the ECM structural parameters including the porosity and fibril radius as reviewed elsewhere [34]. Thus, the capability of quantitatively assessing ECM structures is not only critical to assure quality of engineered tissue but also very useful to predict the various functional properties of tissue without performing various property measurements. The present imaging method may also provide an alternative method to histologic staining to obtain estimates of decellularization effectiveness over a large area.

Besides the research and scientific usages, the proposed imaging method is highly relevant to quality control of cell/tissue engineering products in industrial and clinical settings. As tissue engineering technology advances, a wide variety of engineered tissue have been developed. These include both normal and malignant tissue to replace diseased tissue, to investigate physiology or pathology, and to test new drugs and therapies [35–37]. However, there is currently no reliable method capable of quickly examining a large number of engineered tissues, in which structures are becoming more complex and heterogeneous spatiotemporally. Moreover, a reliable preservation technology is highly needed to scale up tissue engineering from the laboratory scale to the manufacturing scale in order to achieve more effective storage, banking, as well as transportation of tissue engineering products. Cryopreservation is one of the leading candidates to provide this capability. To cryopreserve functional tissue, its ECM microstructures should be maintained during/after cryopreservation. Post-thaw structural changes of both native and engineering tissues after cryopreservation have been reported [7,38–40]. In these studies, even cryopreservation with cryoprotective agents could alter the ECM microstructure of various tissues. If a relevant characterization method is available, it would be useful to develop and optimize successful cryopreservation protocols for various types of tissue, and assess the quality of cryopreservated tissues. In this respect, the spectroscopic imaging method could potentially address these challenges by providing a new high-throughput screening capability of spatiotemporal changes in ECM structures with a great flexibility. Although the F/T protocol used in the present study may be too simple to simulate F/T of cryopreservation protocols, it could create the ECM structural change relevant to cryopreservation. However, further verification with fully cryoperserved tissue samples is necessary.

There are numerous characterization methods to assess ECM structures, in particular pore sizes, of engineered tissue in different length scales [41]. Among other methods, electron microscopy (e.g., SEM and TEM), atomic force microscopy (AFM), small angle X-ray/neutron scattering, swelling methods [42,43], poroelastic methods [44], and particle (e.g., dextran) uptake methods [45] have commonly been used as traditional methods in the fields of tissue engineering and regenerative medicine. The orientation and alignment of collagen fibers in tissue scaffolds/constructs have been characterized by quantitatively assessing birefringence properties [46–48]. Recently, several optical methods have received considerable attention. For example, second harmonic generation (SHG) and multiphoton microscopy have been shown to be useful for visualize ECM structures without relying on staining and labeling [49–53]. It should be noted that SHG and two-photon signals can be applied only to collagen network microstructures. Using 3D data sets of collagen networks from confocal microscopy, a robust pore size analysis method was also developed using fluorescent staining [54]. Optical coherence tomography and microscopy have successfully been used to image ECM microstructures [55–59]. In addition, ultrasound backscatter microscopy has been used to evaluate cartilage constructs cultured in scaffolds [60,61]. Overall, although these methods are valuable for investigating various aspects of ECM structures in small samples, nondestructive, quantitative, whole-field characterization methods are currently lacking.

Although other commonly used characterization methods (e.g., SEM, TEM, AFM, and X-ray diffraction) are highly valuable for investigating various aspects of nanostructures and microstructures of ECM, they do not allow structural characterization over a fairly large area, due to the intrinsic tradeoff between the resolution and the field of view. In addition, these methods require intensive sample preparation, which are sometimes invasive. On the other hand, optical microscopic methods still provide limited sampling at selected points. For example, to image an area of $\sim 30\,\text{mm} \times 30\,\text{mm}$, a field of view (e.g., 0.3 mm) of a conventional microscope would require $\sim$10,000 microscopic images. It should be noted that small angle light scattering approaches can provide detailed structural information as a point-measurement. However, the present imaging method can easily be distinguished because it offers visualization of x–y spatial variations (i.e., imaging) and spectral measurements carry rich structural information, compared with angular measurements [20,21]. In this respect, the present imaging method has two unique features. These are (i) whole-field assessment of ECM structures and (ii) nondestructive quantification of ECM structures. The present method can allow whole-field assessments of ECM structures in an area of $\sim 15\,\text{mm} \times 15\,\text{mm}$, while the spectroscopic measurements provide the information on detailed ECM structures at each (x, y) location. Since it is based on interactions of light with ECM structures, the method does not require any labeling or staining using contrast agents. In addition, the present method is a new application of elastic light scattering to nondestructively assess the ECM structures in engineered tissue scaffolds/constructs.

The proposed imaging method utilizes an elastic light scattering-based approach to visualize ECM microstructures in a large area in engineered tissue. The principle of this method is that the wavelength pattern of light elastically reflected from tissue is determined by the composition and structures of light scatterers [62–64]. Historically, spectral patterns of elastic light scattering were first used to detect carcinoma from the bladder and adenocarcinoma of the colon [12,65]. Oscillatory spectral and angular scattering patterns were successfully used to extract the size distribution of cell nuclei [65,66]. Further, by combining the wavelength and angular scattering properties, this elastic light scattering method was used to detect precancerous alterations from the epithelia. Importantly, the spectral pattern backscattered from biological tissue can capture nanoscale structural alterations in native tissue. In this current study, we have successfully adapted this approach to develop a practical imaging method for rapidly quantifying ECM microstructures in engineered tissue.

Conclusion

We have successfully developed elastic light scattering-based approaches to characterize ECM microstructures in tissue scaffolds and constructs. The present results suggest that the spectral decay rate of light elastically backscattered from engineered tissue can be strongly associated with porous ECM microstructures. We have further shown that the spectroscopic imaging method can capture spatial and temporal alterations in ECM microstructures resulting from fibroblast-embedded collagen gel contraction. Although more quantitative comparisons with conventional methods (e.g., SEM) and detailed origins of the light scattering signals are needed, it shows the feasibility to nondestructively visualize spatial heterogeneity of ECM structures in tissue scaffolds and constructs in a relatively large area. The present imaging method can be extended to a variety of applications, in which either high spatial resolution or high-throughput assessment are required. In particular, the main advantage of the present method is the capability of rapid and noninvasive characterization of engineered tissues and/or scaffolds without labeling or staining. This aspect of this method will be highly relevant to industrial applications, in which simple and rapid quality assessment with high throughput is desired.

Acknowledgment

This study was supported in part by grants from NIH (R03 CA153982 and R21 ES020965 to YLK, and R01 EB008388 to BH). The scanning electron microscopy was performed at Purdue Life Science Microscopy Facility.

References

[1] Lutolf, M. P., and Hubbell, J. A., 2005, "Synthetic Biomaterials as Instructive Extracellular Microenvironments for Morphogenesis in Tissue Engineering," Nat. Biotechnol., **23**, pp. 47–55.
[2] Badylak, S. F., Freytes, D. O., and Gilbert, T. W., 2009, "Extracellular Matrix as a Biological Scaffold Material: Structure and Function," Acta Biomater., **5**, pp. 1–13.
[3] Teo, K. Y., Dehoyos, T. O., Dutton, J. C., Grinnell, F., and Han, B., 2011, "Effects of Freezing-Induced Cell-Fluid-Matrix Interactions on the Cells and Extracellular Matrix of Engineered Tissues," Biomaterials, **32**, pp. 5380–5390.
[4] Badylak, S. F., Taylor, D., and Uygun, K., 2011, "Whole-Organ Tissue Engineering: Decellularization and Recellularization of Three-Dimensional Matrix Scaffolds," Annu. Rev. Biomed. Eng., **13**, pp. 27–53.
[5] Crapo, P. M., Gilbert, T. W., and Badylak, S. F., 2011, "An Overview of Tissue and Whole Organ Decellularization Processes," Biomaterials, **32**, pp. 3233–3243.
[6] Daley, W. P., Peters, S. B., and Larsen, M., 2008, "Extracellular Matrix Dynamics in Development and Regenerative Medicine," J. Cell Sci., **121**, pp. 255–264.
[7] Han, B., Teo, K. Y., Ghosh, S., Dutton, J. C., and Grinnell, F., 2013, "Thermomechanical Analysis of Freezing-Induced Cell-Fluid-Matrix Interactions in Engineered Tissues," J. Mech. Behav. Biomed. Mater., **18**, pp. 67–80.
[8] Kim, Y. L., Liu, Y., Wali, R. K., Roy, H. K., Goldberg, M. J., Kromin, A. K., Chen, K., and Backman, V., 2003, "Comprehensive Description of Light Scattering by Simultaneous Measurement of Angular, Spectral, and Polarization Dependence for Characterization of Tissue Microarchitecture in Normal and Precancerous States," Proc. SPIE, **5141**, pp. 95–105.
[9] Van De Hulst, H. C., 1995, *Light Scattering by Small Particles*, Dover Publications, New York.
[10] Roy, H. K., Kim, Y. L., Wali, R. K., Liu, Y., Koetsier, J., Kunte, D. P., Goldberg, M. J., and Backman, V., 2005, "Spectral Markers in Preneoplastic Intestinal Mucosa: An Accurate Predictor of Tumor Risk in the Min Mouse," Cancer Epidemiol. Biomarkers Prev., **14**, pp. 1639–1645.
[11] Gurjar, R. S., Backman, V., Perelman, L. T., Georgakoudi, I., Badizadegan, K., Itzkan, I., Dasari, R. R., and Feld, M. S., 2001, "Imaging Human Epithelial Properties With Polarized Light-Scattering Spectroscopy," Nat. Med., **7**, pp. 1245–1248.
[12] Roy, H. K., Liu, Y., Wali, R. K., Kim, Y. L., Kromine, A. K., Goldberg, M. J., and Backman, V., 2004, "Four-Dimensional Elastic Light-Scattering Fingerprints as Preneoplastic Markers in the Rat Model of Colon Carcinogenesis," Gastroenterology, **126**, pp. 1071–1081.
[13] Xu, Z., Sun, X., Liu, J., Song, Q., Muckley, M., Akkus, O., and Kim, Y. L., 2010, "Spectroscopic Visualization of Nanoscale Deformation in Bone: Interaction of Light With Partially Disordered Nanostructure," J. Biomed. Opt., **15**, p. 060503.
[14] Han, B., Miller, J. D., and Jung, J. K., 2009, "Freezing-Induced Fluid-Matrix Interaction in Poroelastic Material," ASME J. Biomech. Eng., **131**(2), p. 021002.
[15] Teo, K. Y., Dutton, J. C., and Han, B., 2010, "Spatiotemporal Measurement of Freezing-Induced Deformation of Engineered Tissues," ASME J. Biomech. Eng., **132**(3), p. 031003.
[16] Xu, Z., Liu, J., Hong, D. H., Nguyen, V. Q., Kim, M. R., Mohammed, S. I., and Kim, Y. L., 2010, "Back-Directional Gated Spectroscopic Imaging for Diffuse Light Suppression in High Anisotropic Media and Its Preclinical Applications for Microvascular Imaging," IEEE J. Sel. Top. Quantum Electron., **16**, pp. 815–823.
[17] Xu, Z., Liu, J., and Kim, Y. L., 2009, "Diffuse Light Suppression of Back-Directional Gating Imaging in High Anisotropic Media," J. Biomed. Opt., **14**, p. 030510.
[18] Hunter, M., Backman, V., Popescu, G., Kalashnikov, M., Boone, C. W., Wax, A., Gopal, V., Badizadegan, K., Stoner, G. D., and Feld, M. S., 2006, "Tissue Self-Affinity and Polarized Light Scattering in the Born Approximation: A New Model for Precancer Detection," Phys. Rev. Lett., **97**, p. 138102.
[19] Han, B., Teo, K. Y., Ghosh, S., Dutton, J. C., and Grinnell, F., 2013, "Thermomechanical Analysis of Freezing-Induced Cell-Fluid-Matrix Interactions in Engineered Tissues," J. Mech. Behav. Biomed. Mater., **18**, pp. 67–80.
[20] Subramanian, H., Pradhan, P., Liu, Y., Capoglu, I. R., Li, X., Rogers, J. D., Heifetz, A., Kunte, D., Roy, H. K., Taflove, A., and Backman, V., 2008, "Optical Methodology for Detecting Histologically Unapparent Nanoscale Consequences of Genetic Alterations in Biological Cells," Proc. Natl. Acad. Sci. USA, **105**, pp. 20118–20123.
[21] Qiu, L., Pleskow, D. K., Chuttani, R., Vitkin, E., Leyden, J., Ozden, N., Itani, S., Guo, L. Y., Sacks, A., Goldsmith, J. D., Modell, M. D., Hanlon, E. B., Itzkan, I., and Perelman, L. T., 2010, "Multispectral Scanning During Endoscopy Guides Biopsy of Dysplasia in Barrett's Esophagus," Nat. Med., **16**, pp. 603–606.
[22] Konger, R. L., Xu, Z., Sahu, R. P., Rashid, B. M., Mehta, S. R., Mohamed, D. R., Dasilva-Arnold, S. C., Bradish, J. R., Warren, S. J., and Kim, Y. L., 2013, "Spatiotemporal Assessments of Dermal Hyperemia Enable Accurate Prediction of Experimental Cutaneous Carcinogenesis as Well as Chemopreventive Activity," Cancer Res., **73**, pp. 150–159.
[23] Prahl, S. A., Van Gemert, M. J. C., and Welch, A. J., 1993, "Determining the Optical Properties of Turbid Media by Using the Adding Doubling Method," Appl. Opt., **32**, pp. 559–568.
[24] Jiang, H., and Grinnell, F., 2005, "Cell-Matrix Entanglement and Mechanical Anchorage of Fibroblasts in Three-Dimensional Collagen Matrices," Mol. Biol. Cell, **16**, pp. 5070–5076.
[25] Panwar, P., Du, X., Sharma, V., Lamour, G., Castro, M., Li, H., and Bromme, D., 2013, "Effects of Cysteine Proteases on the Structural and Mechancial Properties of Collagen Fibers," J. Biol. Chem., **288**, pp. 5940–5950.
[26] Varani, J., Perone, P., Deming, M. O., Warner, R. L., Asiam, M. N., Bhagavathula, N., Dame, M. K., and Voorhees, J. J., 2009, "Impaired Keratinocyte Function on Matrix Metalloproteinase-1 (Mmp-1) Damaged Collagen," Arch. Dermatol. Res., **301**, pp. 497–506.
[27] Tamariz, E., and Grinnell, F., 2002, "Modulation of Fibrolbast Morphology and Adhesion During Collagen Matrix Remodeling," Mol. Biol. Cell, **13**, pp. 3915–3929.
[28] Grinnell, F., 2000, "Fibroblast-Collagen Matrix Contraction: Growth-Factor Signalling and Mechanical Loading," Trends Cell Biol., **10**, pp. 362–365.
[29] O'Brien, F. J., Harley, B. A., Waller, M. A., Yannas, I. V., Gibson, L. J., and Prendergast, P. J., 2007, "The Effect of Pore Size on Permeability and Cell Attachment in Collagen Scaffolds for Tissue Engineering," Technol. Health Care, **15**, pp. 3–17.
[30] Mackie, J. S., and Meares, P., 1955, "The Diffusion of Electrolytes in a Cation-Exchange Resin Membrane," Proc. R. Soc. London, Ser. A, **232**, pp. 498–509.
[31] Wang, J. H., 1954, "Theory of the Self-Diffusion of Water in Protein Solutions. A New Method for Studying the Hydration and Shape of Protein Molecules," J. Am. Chem. Soc., **76**, pp. 4755–4763.
[32] Clague, D. S., and Phillips, R. J., 1996, "Hindered Diffusion of Spherical Macromolecules Through Dilute Fibrous Media," Phys. Fluids, **8**, pp. 1720–1731.
[33] Johnson, E. M., Berk, D. A., Jain, R. K., and Deen, W. M., 1996, "Hindered Diffusion in Agarose Gels: Test of Effective Medium Model," Biophys. J., **70**, pp. 1017–1026.
[34] Phillips, R. J., 2000, "A Hydrodynamic Model for Hindered Diffusion of Proteins and Micelles in Hydrogels," Biophys. J., **79**, pp. 3350–3354.
[35] Griffith, L. G., and Swartz, M. A., 2006, "Capturing Complex 3D Tissue Physiology In Vitro," Nat. Rev. Mol. Cell Biol., **7**, pp. 211–224.
[36] Kim, J. B., Stein, R., and O'Hare, M. J., 2004, "Three-Dimensional In Vitro Tissue Culture Models of Breast Cancer—A Review," Breast Cancer Res. Treat., **85**, pp. 281–291.
[37] Han, B., Grassl, E., Barocas, V., Coad, J., and Bischof, J. C., 2005, "A Cryoinjury Modeling Using Engineered Tissue Equivalents for Cryosurgical Applications," Ann. Biomed. Eng., **33**, pp. 980–990.
[38] Schenke-Layland, K., Madershahian, N., Riemann, I., Starcher, B., Halbhuber, K. J., Konig, K., and Stock, U. A., 2006, "Impact of Cryopreservation on Extracellular Matrix Structures of Heart Valve Leaflets," Ann. Thorac. Surg., **81**, pp. 918–926.
[39] Schenke-Layland, K., Xie, J., Heydarkhan-Hagvall, S., Hamm-Alvarez, S. F., Stock, U. A., Brockbank, K. G., and MacLellan, W. R., 2007, "Optimzied Preservation of Extracellular Matrix in Cardiac Tissues: Implication for Long-Term Graft Durability," Ann. Thorac. Surg., **83**, pp. 1641–1650.
[40] Venkatasubramanian, R. T., Grassl, E. D., Barocas, V. H., Lafontaine, D., and Bischof, J. C., 2006, "Effects of Freezing and Cryopreservation on the Mechanical Properties of Arteries," Ann. Biomed. Eng., **34**, pp. 823–832.
[41] Tomlins, P., Grant, P., Mikhalovsky, S., James, S., and Mikhalovska, L., 2004, "Measurement of Pore Size and Porosity of Tissue Scaffolds," J. ASTM Int., **1**, p. JAI11510.
[42] Canal, T., and Peppas, N. A., 1989, "Correlation Between Mesh Size and Equilibrium Degree of Swelling of Polymeric Networks," J. Biomed. Mater. Res., **23**, pp. 1183–1193.
[43] Cruise, G. M., Scharp, D. S., and Hubbell, J. A., 1998, "Characterization of Permeability and Network Structure of Interfacially Photopolymerized Poly(Ethylene Glycol) Diacrylate Hydrogels," Biomaterials, **19**, pp. 1287–1294.
[44] Strange, D. G. T., and Oyen, M. L., 2012, "Composite Hydrogels for Nucleus Pulposus Tissue Engineering," J. Mech. Behav. Biomed. Mater., **11**, pp. 16–26.
[45] Li, Y. A., Kleijn, J. M., Stuart, M. A. C., Slaghek, T., Timmermans, J., and Norde, W., 2011, "Mobility of Lysozyme Inside Oxidized Starch Polymer Microgels," Soft Matter, **7**, pp. 1926–1935.
[46] Tower, T. T., and Tranquillo, R. T., 2001, "Alignment Maps of Tissues: II. Fast Harmonic Analysis for Imaging," Biophys. J., **81**, pp. 2964–2971.
[47] Chandran, P. L., and Barocas, V. H., 2004, "Microstructural Mechanics of Collagen Gels in Confined Compression: Poroelasticity, Viscoelasticity, and Collapse," ASME J. Biomech. Eng., **126**(2), pp. 152–166.
[48] Quinn, K. P., and Winkelstein, B. A., 2010, "Full Field Strain Measurements of Collagenous Tissue by Tracking Fiber Alignment Through Vector Correlation," J. Biomech., **43**, pp. 2637–2640.
[49] Zoumi, A., Yeh, A., and Tromberg, B. J., 2002, "Imaging Cells and Extracellular Matrix In Vivo by Using Second-Harmonic Generation and Two-Photon Excited Fluorescence," Proc. Natl. Acad. Sci. USA, **99**, pp. 11014–11019.
[50] Raub, C. B., Unruh, J., Suresh, V., Krasieva, T., Lindmo, T., Gratton, E., Tromberg, B. J., and George, S. C., 2008, "Image Correlation Spectroscopy of Multiphoton Images Correlates With Collagen Mechanical Properties," Biophys. J., **94**, pp. 2361–2373.

[51] Raub, C. B., Putnam, A. J., Tromberg, B. J., and George, S. C., 2010, "Predicting Bulk Mechanical Properties of Cellularized Collagen Gels Using Multiphoton Microscopy," Acta Biomater., **6**, pp. 4657–4665.
[52] Xylas, J., Alt-Holland, A., Garlick, J., Hunter, M., and Georgakoudi, I., 2010, "Intrinsic Optical Biomarkers Associated With the Invasive Potential of Tumor Cells in Engineered Tissue Models," Biomed. Opt. Express, **1**, pp. 1387–1400.
[53] Ajeti, V., Nadiarnykh, O., Ponik, S. M., Keely, P. J., Eliceiri, K. W., and Campagnola, P. J., 2011, "Structural Changes in Mixed Col I/Col V Collagen Gels Probed by SHG Microscopy: Implications for Probing Stromal Alterations in Human Breast Cancer," Biomed. Opt. Express, **2**, pp. 2307–2316.
[54] Mickel, W., Munster, S., Jawerth, L. M., Vader, D. A., Weitz, D. A., Sheppard, A. P., Mecke, K., Fabry, B., and Schroder-Turk, G. E., 2008, "Robust Pore Size Analysis of Filamentous Networks From Three-Dimensional Confocal Microscopy," Biophys. J., **95**, pp. 6072–6080.
[55] Chen, C. W., Betz, M. W., Fisher, J. P., Paek, A., and Chen, Y., 2011, "Macroporous Hydrogel Scaffolds and Their Characterization by Optical Coherence Tomography," Tissue Eng. Part C-Methods, **17**, pp. 101–112.
[56] Jia, Y. L., Bagnaninchi, P. O., Yang, Y., El Haj, A., Hinds, M. T., Kirkpatrick, S. J., and Wang, R. K. K., 2009, "Doppler Optical Coherence Tomography Imaging of Local Fluid Flow and Shear Stress Within Microporous Scaffolds," J. Biomed. Opt., **14**, p. 034014.
[57] Patterson, J., Stayton, P. S., and Li, X. D., 2009, "In Situ Characterization of the Degradation of PLGA Microspheres in Hyaluronic Acid Hydrogels by Optical Coherence Tomography," IEEE Trans. Med. Imaging, **28**, pp. 74–81.
[58] Wang, Z. G., Pan, H., Yuan, Z. J., Liu, J. X., Chen, W. L., and Pan, Y. T., 2008, "Assessment of Dermal Wound Repair After Collagen Implantation With Optical Coherence Tomography," Tissue Eng. Part C-Methods, **14**, pp. 35–45.
[59] Gomez-Lara, J., Brugaletta, S., Diletti, R., Garg, S., Onuma, Y., Gogas, B. D., Van Geuns, R. J., Dorange, C., Veldhof, S., Rapoza, R., Whitbourn, R., Windecker, S., Garcia-Garcia, H. M., Regar, E., and Serruys, P. W., 2011, "A Comparative Assessment by Optical Coherence Tomography of the Performance of the First and Second Generation of the Everolimus-Eluting Bioresorbable Vascular Scaffolds," Eur. Heart J., **32**, pp. 294–304.
[60] Kreitz, S., Dohmen, G., Hasken, S., Schmitz-Rode, T., Mela, P., and Jockenhoevel, S., 2011, "Nondestructive Method to Evaluate the Collagen Content of Fibrin-Based Tissue Engineered Structures via Ultrasound," Tissue Eng. Part C-Methods, **17**, pp. 1021–1026.
[61] Sun, Y., Responte, D., Xie, H., Liu, J., Fatakdawala, H., Hu, J., Athanasiou, K., and Marcu, L., 2012, "Nondestructive Evaluation of Tissue Engineered Articular Cartilage Using Time-Resolved Fluorescence Spectroscopy and Ultrasound Backscatter Microscopy," Tissue Eng. Part C-Methods, **18**, pp. 215–226.
[62] Perelman, L. T., 2006, "Optical Diagnostic Technology Based on Light Scattering Spectroscopy for Early Cancer Detection," Expert Rev. Med. Devices, **3**, pp. 787–803.
[63] Boustany, N. N., Boppart, S. A., and Backman, V., 2010, "Microscopic Imaging and Spectroscopy With Scattered Light," Annu. Rev. Biomed. Eng., **12**, pp. 285–314.
[64] Bigio, I. J., and Mourant, J. R., 1997, "Ultraviolet and Visible Spectroscopies for Tissue Diagnostics: Fluorescence Spectroscopy and Elastic-Scattering Spectroscopy," Phys. Med. Biol., **42**, pp. 803–814.
[65] Backman, V., Wallace, M. B., Perelman, L. T., Arendt, J. T., Gurjar, R., Muller, M. G., Zhang, Q., Zonios, G., Kline, E., McGillican, T., Shapshay, S., Valdez, T., Badizadegan, K., Crawford, J. M., Fitzmaurice, M., Kabani, S., Levin, H. S., Seiler, M., Dasari, R. R., Itzkan, I., Van Dam, J., and Feld, M. S., 2000, "Detection of Preinvasive Cancer Cells," Nature, **406**, pp. 35–36.
[66] Perelman, L. T., Backman, V., Wallace, M., Zonios, G., Manoharan, R., Nusrat, A., Shields, S., Seiler, M., Lima, C., Hamano, T., Itzkan, I., Van Dam, J., Crawford, J. M., and Feld, M. S., 1998, "Observation of Periodic Fine Structure in Reflectance From Biological Tissue: A New Technique for Measuring Nuclear Size Distribution," Phys. Rev. Lett., **80**, pp. 627–630.